

Boosting Oxygen and Peroxide Reduction Reactions on PdCu Intermetallic Cubes

Qingfeng Zhang,^[a] Fan Li,^[a] Lina Lin,^[b] Jiaheng Peng,^[a] Wencong Zhang,^[a] Wenlong Chen,^[a] Qian Xiang,^[a] Fenglei Shi,^[a] Wen Shang,^[a] Peng Tao,^[a] Chengyi Song,^[a] Rong Huang,^{*,[b]} Hong Zhu,^[a, c, d] Tao Deng,^[a, d, e] and Jianbo Wu^{*,[a, d, e]}

Palladium-based nanocatalysts have the potential to replace platinum-based catalysts for fuel-cell reactions in alkaline electrolytes, especially PdCu intermetallic nanoparticles with high electrochemical activity and stability. However, unlike the synthetic methods for obtaining the nanoparticles, the effect of PdCu shape on the performance is relatively less well studied. Here, we demonstrate the facet dependence of PdCu intermetallics on the oxygen reduction reaction (ORR) and peroxide reduction, and reveal that the {100} dominant PdCu cubes have a much higher ORR mass activity and specific activity than spheres at 0.9 V vs. RHE, which is four and five times that of

commercial Pd/C and Pt/C catalysts, respectively, and show only a 31.7% decay after 30000 cycles in the stability test. Moreover, cubic PdCu nanoparticles show higher peroxide electroreduction activity than Pd cubes and PdCu spheres. Density functional theory (DFT) calculation reveals that the huge difference originates from the reduction in oxygen adsorption energy and energy barrier of peroxide decomposition on the ordered {100} PdCu surface. Given the relationship between the shape and electrochemical performance, this study will contribute to further research on electrocatalytic improvements of catalysts in alkaline environments.

1. Introduction

The platinum-based catalysts are highly pivotal for the electrochemical reactions,^[1] especially for the sluggish oxygen reduction reaction in proton exchange membrane fuel cell (PEMFC),^[2,3] Many researchers focused on the boosts of the activity,^[4,5] and durability,^[6,7] of these catalysts by morphology,^[8–10] and composition engineering. However, the scarce world reserves, high cost and poor long-term duration restrict their wide applications.^[11] Besides, the major problem

with platinum-group metals is the low activity in alkaline environment because of the difficulty in achieving the optimized oxygen binding strength in the presence of hydroxide.^[12] Among the other noble metal catalysts, Pd and Pd-based alloys can become the promising electrocatalysts in alkaline environment.^[13–15] The other oxygen relevant electrochemical reaction, hydrogen peroxide electroreduction, can also be powered by Pd-based catalysts.^[16] The hydrogen peroxide plays an important role in the living cells and its concentration at the normal level can maintain the health of the living body.^[17] In the previous studies, Pt and Pt-based nanocomposites were widely used for catalysts.^[18] To reduce its cost, Pd-based nanocatalysts were investigated and showed impressive performance, such as PdPt,^[19] PtPd–Fe₃O₄,^[20] Pd–Au.^[16] In order to reduce the cost, the cheaper nanocatalysts, PdCu, may show its potential in this reaction.

The catalytic activity of noble metals can be improved through alloying by achieving the optimized oxygen binding strength. In recent years, many Pd-based catalysts have been reported with the catalytic performance comparable to or even superior to that of the commercial Pt/C, such PdNi,^[21] PdCo,^[22] PdFe,^[23,24] PdW,^[25] and PdCu.^[26] Among these bimetallic nanocatalysts, the PdCu alloys received much attention for their high electrochemical activity and low cost.^[27,28] Many efforts have been focused on the control of the size, composition, shape and structure to boost its ORR activity.^[29–32] However, previous studies mainly focused on its A1 phase with disordered structure. Such random alloy suffers from poorer stability compared with Pt-based nanocrystals in corrosive environment. Different with the conventional disordered structure, the ordered structure with fixed atom positions and site occupancies shows great enhanced

[a] Q. Zhang, F. Li, J. Peng, W. Zhang, Dr. W. Chen, Q. Xiang, F. Shi, Prof. W. Shang, Prof. P. Tao, Prof. C. Song, Prof. H. Zhu, Prof. T. Deng, Prof. J. Wu

State Key Laboratory of Metal Matrix Composites
School of Materials Science and Engineering
Shanghai Jiao Tong University
800 Dongchuan Rd, Shanghai, 200240, China
E-mail: jianbowu@sjtu.edu.cn


[b] L. Lin, Prof. R. Huang
Key Laboratory of Polar Materials and Devices (MOE) and Department of Electronics

East China Normal University
Shanghai 200062, China
E-mail: rhuang@ee.ecnu.edu.cn

[c] Prof. H. Zhu
University of Michigan – Shanghai Jiao Tong University Joint Institute
Shanghai Jiao Tong University
800 Dongchuan Road, Shanghai, 200240, China

[d] Prof. H. Zhu, Prof. T. Deng, Prof. J. Wu
Materials Genome Initiative Center
Shanghai Jiao Tong University
800 Dongchuan Road, Shanghai 200240, China

[e] Prof. T. Deng, Prof. J. Wu
Center of Hydrogen Science
Shanghai Jiao Tong University
800 Dongchuan Road, Shanghai 200240, China

 Supporting information for this article is available on the WWW under <https://doi.org/10.1002/celec.202000381>

stability due to the formation of uniform heteroatomic bonding.^[33,34]

Inspired by this, the ordered B2 phase of PdCu with intermetallic structure was engineered to achieve this prospect by the seed-mediated co-reduction route,^[35] high temperature annealing^[36,37] or one-step liquid reduction method.^[38,39] Very few works could synthesize the faceted PdCu intermetallics regarding both durability and activity. Recently, Sara E. Skrabalak et al. have reported the enhanced activity and stability for oxygen reduction reaction of PdCu intermetallic cube compared with the random alloy.^[35,40] Nevertheless, few studies have reported the comparison of PdCu ordered alloys with different shapes in electrochemical performance and explained the origin of the enhancement of the oriented ordering on performance.

In this work, we successfully synthesized two shapes of PdCu intermetallics, cubes and spheres, by slightly modifying the reported method^[41] and investigated the effect of facet and ordering on their electrochemical properties in both ORR and hydrogen peroxide reduction reaction. The PdCu cube/C shows the large improvements in both ORR and peroxide reduction. The PdCu cube shows up to 5 times improvements in mass activity towards ORR while the PdCu sphere just shows almost the same activity compared with the commercial Pt/C catalysts. For H₂O₂ reduction, the PdCu cube shows the enhancements of up to 8.4 times for mass activity compared with the PdCu sphere. The DFT calculation reveals that huge difference originates from the reduction of oxygen adsorption energy and energy barrier of peroxide decomposition on order {100} PdCu surface.

2. Results and Discussion

2.1. Nanoparticle Synthesis and Structural Characterization

Two catalysts for comparison were prepared by the same capping reagent (TPP) with different amounts. The size and Pd-to-Cu ratio of two particles remained nearly constant in order to compare the shape-induced difference (Figure 1 and Table S1).

Figure 1a and Figure 1b show the monodisperse PdCu intermetallic nanocubes and nanospheres with an average size of 11.57 nm and 10.58 nm, respectively. HAADF-STEM, HRTEM and XRD were utilized to confirm the ordered PdCu structure. The atomic spacing of 0.297 nm and 0.210 nm in the STEM image of a single PdCu nanocube (inset in Figure 1a) and HR-TEM image of a single nanosphere (inset in Figure 1b) are corresponding to the (100) and (110) plane of PdCu B2 phase,^[42] respectively, which is consistent with the (100) and (110) spacings from XRD pattern (Figure 1e).

From the EDS mapping (Figure 1c and Figure 1d), the Pd and Cu elements distribute uniformly, which confirms the formation of PdCu alloy. The cubic and spherical PdCu nanocrystals were evaluated by ICP, indicating that Pd and Cu were almost identical in content (Table S1), which is

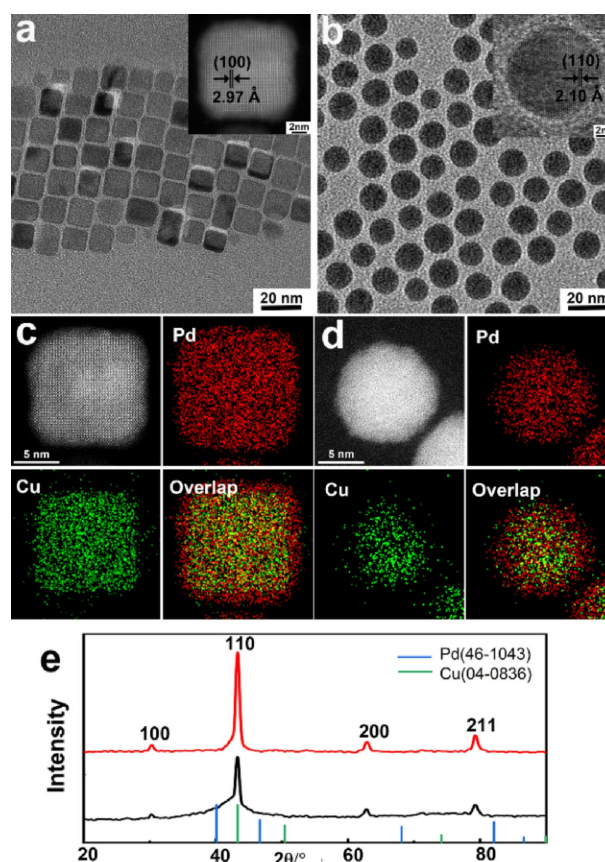


Figure 1. Characterization of morphology and composition of PdCu nanoparticles. TEM images of a) cubes b) spheres. Insets: a) atomic-resolution HAADF-STEM images of PdCu cubes and b) HR-TEM image of PdCu spheres. EDS mappings of c) cubes and d) spheres. e) XRD patterns of PdCu cubes and spheres.

consistent with the elemental ratio of PdCu B2 ordered phase.

The temperature played a significant part in the synthesis of cubic PdCu nanoparticles. The monodisperse PdCu nanocubes could be obtained at 170 °C. When heated to 180 °C and 200 °C, some of cubes would turn into spheres due to the weak control of capping agent on the diffusion of Pd and Cu atoms at higher temperature (Figure S1a and Figure S1b). Thus, the final product was composed of nearly 100% spheres with size of 18 nm when the temperature reached 220 °C, indicating the capping reagent lost its shape-controlled ability completely because of the rapid diffusion rate (Figure S1c)

2.2. Electrochemical Evaluation

To investigate the differences in electrochemical performance of these two PdCu nanocatalysts, the ORR and hydrogen peroxide reduction reaction were both tested.

Around 10 nm Pd cubes prepared by reported method^[43] (Figure S2), the commercial Pt/C and Pd/C were used for comparative studies. The CV tests were taken to activate the

surface of catalysts before the electrochemical measurement (Figure S3). The electrochemical active surface areas (ECSA) of Pd-based catalysts were calculated by CO stripping method,^[44,45] except the commercial Pt/C, that of which was determined by integrating hydrogen adsorption-desorption region in the cyclic voltammetry (CV) curves (Figure S3–S9). The PdCu cubes and spheres exhibit the ECSA of $59.4 \text{ m}^2 \text{ g}^{-1}_{\text{Pd}}$ and $39.4 \text{ m}^2 \text{ g}^{-1}_{\text{Pd}}$, which are comparable to that of the commercial Pt/C ($63.2 \text{ m}^2 \text{ g}^{-1}_{\text{Pt}}$).

ORR measurements were carried out by rotating disk electrodes (RDE) in the 0.1 M O_2 -saturated KOH solution. The LSV curves are shown in Figure 2a. The PdCu B2 cube/C shows a slightly higher onset (0.941 V) and half-wave potential (0.896 V) than Pd cube/C, much higher than PdCu sphere/C, commercial Pt/C and Pd/C catalysts. Figure 2b compares the specific and mass activities of all the nanocatalysts at 0.9 V (vs. RHE). The specific activity is $0.42 \text{ mA cm}^{-2}_{\text{Pd}}$ for PdCu cube/C, which is slightly higher than that of Pd cube/C ($0.41 \text{ mA cm}^{-2}_{\text{Pd}}$), 3, 4, and 5 times as high as that of PdCu sphere/C ($0.14 \text{ mA cm}^{-2}_{\text{Pd}}$), Pd/C ($0.12 \text{ mA cm}^{-2}_{\text{Pd}}$), and Pt/C ($0.08 \text{ mA cm}^{-2}_{\text{Pd}}$), respectively. The mass activity of PdCu cube/C reaches $0.25 \text{ A mg}^{-1}_{\text{Pd}}$, which is about 28% higher than that of Pd cube/C ($0.18 \text{ A mg}^{-1}_{\text{Pd}}$), 5, 4, and 5 times higher than that of PdCu sphere/C ($0.054 \text{ A mg}^{-1}_{\text{Pd}}$), Pd/C ($0.061 \text{ A mg}^{-1}_{\text{Pd}}$) and Pt/C ($0.056 \text{ A mg}^{-1}_{\text{Pd}}$). The PdCu cube/C performs better than Pd cube/C due to the alloying Cu and contributing to the decrease of oxygen adsorption.^[46] The superior performance of PdCu cube/C than sphere might be ascribed to its advanced PdCu ordered atomic arrangement on PdCu {100}.

The stability of all the catalysts were measured by accelerated durability test (ADT) in Ar-purged 0.1 M KOH (Figure 2c–2d and S10). The negative shifts of the half-wave potential can be observed for PdCu cube/C (13 mV) and PdCu sphere/C (16 mV) in Figure 2c due to the aggregation and etching of particles and change of shapes after 30000 cycles.^[47] The onset potentials also showed the negative shifts of 12 mV for PdCu cube/C and 15 mV for PdCu sphere/C, respectively, which indicates the better stability of PdCu cube compared with that of PdCu sphere. Figure 2d shows that the mass activity of PdCu cube/C decreases to $0.17 \text{ A mg}^{-1}_{\text{Pd}}$ with a loss of 31.7%, which is higher than that of Pd cube/C ($0.10 \text{ A mg}^{-1}_{\text{Pd}}$, 44.6% loss), PdCu sphere/C ($0.03 \text{ A mg}^{-1}_{\text{Pd}}$, 41.3% loss) and Pt/C ($0.02 \text{ A mg}^{-1}_{\text{Pt}}$, 61.4% loss).

Furthermore, the morphologies and compositions of these catalysts after ADT test were also investigated by TEM (Figure S11) and EDS (Figure S12 and Table S1). The morphologies of PdCu cube/C and PdCu sphere/C were maintained after the stability test while the commercial Pt/C and Pd/C catalysts particles aggregated, which largely reduced the durability. The superior durability of intermetallic PdCu catalysts may be ascribed to the ordering atomic arrangement of PdCu nanoparticles.^[40] The PdCu sphere/C showed more leaching of copper component (37.7% remaining) than the PdCu cube/C (42.1% remaining) after the ADT test, which indicated the PdCu intermetallic cube prevented the etching of Cu more than PdCu sphere. This trend might be due to the fact that the low-index PdCu {100} showed fewer surface defects than that on the high-index surface of sphere. Herein,

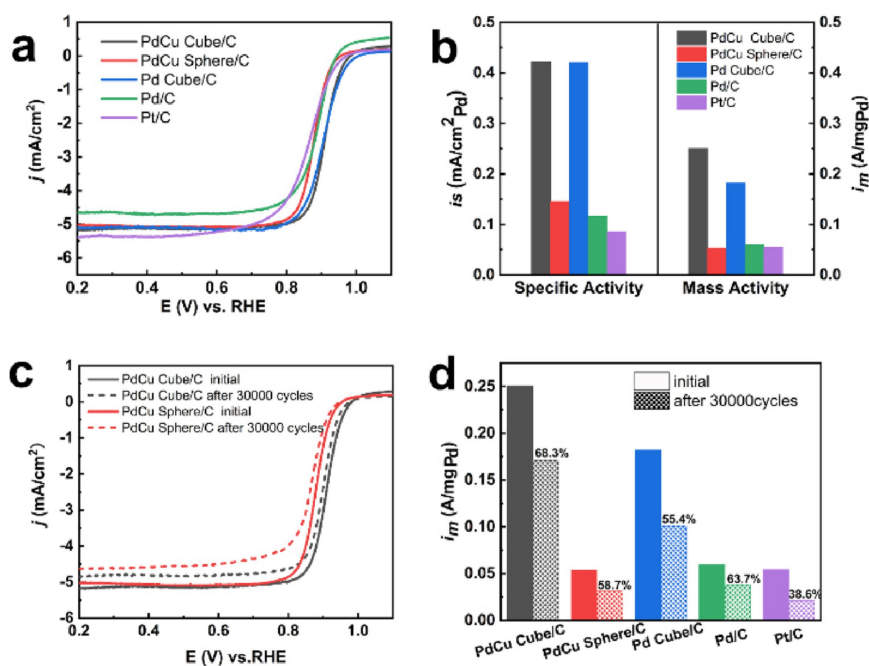


Figure 2. Electro catalytic performance of PdCu cubes, spheres, Pd cubes, commercial Pd/C and Pt/C. ORR polarization curves (a) and comparison of the mass and specific activities (b) of the stated catalysts in 0.1 M KOH at 0.9 V versus RHE. ORR polarization curves (c) and the mass activity change (d) of stated catalyst before and after 30000 cycles.

this protection of Cu from leaching leads to the better durability of PdCu cubes.

It is quite interesting that the PdCu intermetallic cube shows better stability even than Pd cube. From the EDS mapping image (Figure 1c), there is the ultrathin Pd skin on the PdCu cube, making the cube like the core-shell structure. The Pd outlayer is under the tensile strain induced from the different interplanar crystal spacing between PdCu and Pd.^[48,49] The Pd atomic layers near the surface can get closer to each other when stretched, making the surface of this structure denser than that of pure Pd cubes. This tensile strain may enhance the PdCu cubes durability (Figure S13). Although Pd/C only lost 36.3% of initial mass activity, its striking negative shift to half-wave potential and extremely low limited current hinder its application (Figure S10). Thus, the ADT results indicate the PdCu cube/C has the best stability in alkaline environment among the tested samples.

The advantage of PdCu cube/C in H₂O₂ reduction reaction, was conducted in Ar-saturated 0.1 M phosphate buffered saline (PBS). Figure 3a shows the CV curves of PdCu cube/C, PdCu sphere/C and Pd cube/C with and without H₂O₂. The obvious enhanced reduction peak can be observed after addition of H₂O₂, confirming the current is generated by catalytic reduction of H₂O₂.^[20] The reduction peak currents of catalysts were normalized to loading noble metal to compare their mass activity (Figure 3b). The mass activity of PdCu cube/C was 0.042 A mg⁻¹_{Pd}, which is 1.6 times higher than that of Pd cube/C (0.026 A/mg⁻¹_{Pd}) and 8.4 times than that of PdCu sphere/C (0.005 A mg⁻¹_{Pd}). Compared with the

pure Pd cube, the enhanced performance of the PdCu may result from the synergistic effect.^[18] The presence of Cu could increase the adsorption sites for –OH species because it can reduce the strength of Pd–OH formation. The reduction peak current augments when increasing the amount of H₂O₂, further confirming the catalytic ability (Figure 3c). The linear relationship can be obtained according to CV curves when the concentration of H₂O₂ increases from 5 to 25 mM, which suggests its potential as hydrogen peroxide sensor.^[50] Meanwhile, the cathodic peak currents increase when the sweep rate increases (Figure 3d). The linear relationship as the inserted image shows suggests that the H₂O₂ reduction is the typical diffusion-controlled process.^[51]

Based on the previous research,^[52] the oxygen in the oxygen reduction reaction is reduced either directly to the water (four electrons reaction) or to peroxide (two electrons reaction). The latter is preferred on the Pd and Pd-based alloys.^[53]

As discussed in the studies,^[15] the coverage of the hydroxyl species (OH_{ad}) shrinks the activate site for adsorption of oxygen. The superior activity of PdCu cubes can be attributed to low coverage of the OH_{ad}.^[1] The process of adsorption and desorption of oxygen or hydroxyl was found to be the determining step of the ORR.^[54] Thus, the adsorption energy of oxygen or hydroxyl has been used as a descriptor of maximal catalytic activity in the volcano curves of the activity. Generally, the oxygen adsorption energy can be used to evaluate the ORR activity. The closer to the peak of the volcano plot, the higher catalytic activity. To further

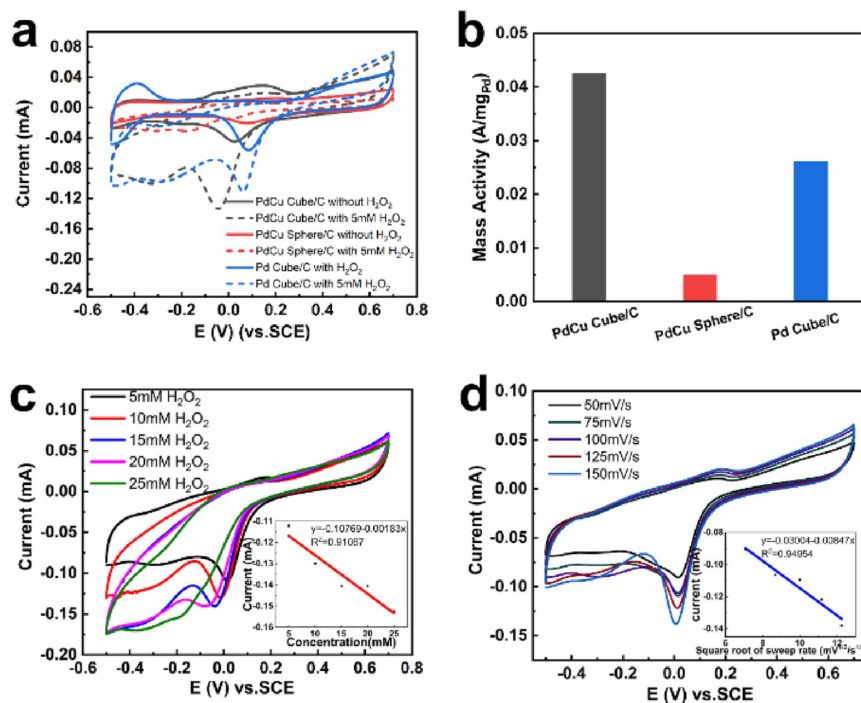


Figure 3. H₂O₂ reduction performance of PdCu cubes, spheres, Pd cubes. CV curves (a) and comparison of the mass activities (b) of the catalysts in 0.1 M PBS solution. CV curves of PdCu cubes in 0.1 M PBS with different H₂O₂ concentration (sweep rate is 100 mV/s), the inset shows the corresponding linear relationship (c). CV curves of PdCu cubes in 0.1 M PBS with 0.5 mM H₂O₂ concentration at different sweep rates, the inset shows the corresponding linear relationship (d).

demonstrate the mechanism, density functional theory (DFT) was used to calculate the oxygen adsorption energy (E_o) that was widely used for measuring the ORR activity (see the details in Supporting information). The PdCu (100) and (110) slabs were built to represent the cubic and spherical PdCu models on the basis of the corresponding HAADF-STEM and HRTEM images (Figure S14).^[55]

We compared the oxygen adsorption energy between the cubic and spherical PdCu particles (Figure 4a and 4b). The E_o of the PdCu cube is -1.082 eV, which is smaller than that of the sphere (-1.182 eV), suggesting that PdCu cubes show higher ORR activity according to the volcano plot in the previous study.^[54]

For peroxide reduction reaction, according to the literature,^[56] the rate-determining step is as follows [Eq. (1)]:



In order to calculate the energy barrier of the rate-determining step of PdCu cubes and spheres, we carried out

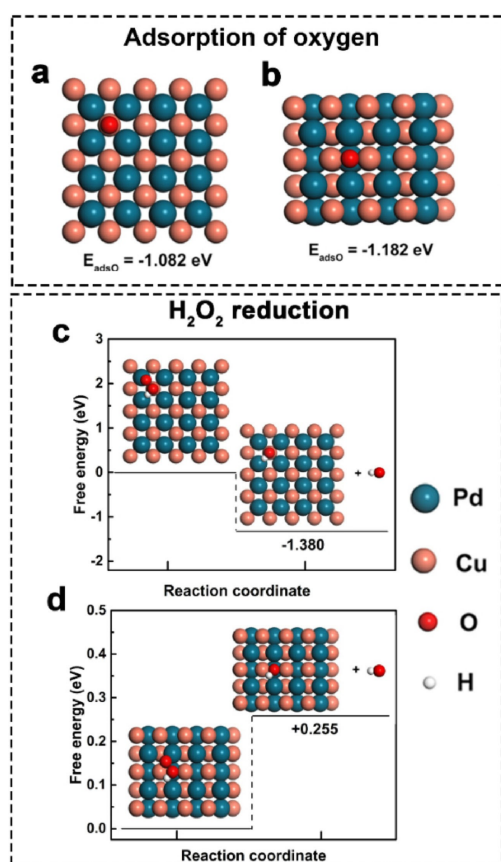


Figure 4. DFT models and results of ORR and H_2O_2 reduction. a) Stable adsorption site of the ORR determining intermediates, O, for PdCu (100) surface slab and the matched binding energy. b) Stable adsorption site of the ORR determining intermediates, O, for PdCu (110) surface slab and the matched binding energy. c) Energy barrier of peroxide reduction reaction's rate-determining step and the stable adsorption configuration of H_2O_2 , left HO on the surface of PdCu (100) slab. d) Energy barrier of peroxide reduction reaction's rate-determining step and the stable adsorption configuration of H_2O_2 , left HO on the surface of PdCu (110) slab.

DFT calculations on the surface of PdCu (100) and (110) slabs. We calculated the corresponding energy barrier to investigate the reason for the improved activity for the peroxide electroreduction (Figure 4c–d). The negative energy barrier for PdCu cubes (-1.380 eV) indicates that the peroxide reduction reaction is more easily to take place on the surface of PdCu cubes compared with that of PdCu spheres (0.255 eV). Thus, the PdCu cubes are thermodynamically favorable for peroxide reduction reaction. Corresponding to the experimental results, our calculation results confirm the shape-induced influence on the electrochemical performance of PdCu particles.

3. Conclusions

We have demonstrated the facet dependence of PdCu intermetallics on ORR and hydrogen peroxides reduction and revealed the {100} dominant PdCu cube shows superior performance than spheres in both ORR and H_2O_2 reduction reaction. Owing to their intermetallic phases, the PdCu cubes exhibit 5 times improved mass activity of and stability with only 31.7% loss after 30000 cycles in ORR and 8.4 times enhancements in H_2O_2 reduction compared to PdCu sphere. DFT calculation has uncovered that the dominant {100} crystal faces in cubes had more appropriate oxygen adsorption and thermodynamically favorable for peroxide reduction than that of spheres. Therefore, our demonstration of the Pd based intermetallics reveals the extended application of Pd based catalysts in the improvements of electro-catalytic performance.

Experimental Section

Materials

Oleylamine (80–90%, OLA), sodium tetrachloropalladate(II) (Na_2PdCl_4 , 99.99%), and triphenylphosphine (TPP, >99.0%, GC) were purchased from Aladdin Industrial Inc. Cupric chloride dehydrate ($\text{CuCl}_2 \cdot 2\text{H}_2\text{O}$, 99.99%) was purchased from Macklin Industrial Inc. Bis(acetylacetonato) palladium (II) ($\text{Pd}(\text{acac})_2$) was purchased from Chengdu Boon Stream Chemical Industry Co. Ltd. Toluene (AR) and potassium bromide (KBr, AR) were purchased from Sinopharm group chemical reagent co. LTD. N-butylamine (>90%) was obtained from TCI reagent company. 5 wt.% Nafion solution, Perchloric acid (HClO_4 , 99.999%), Ascorbic acid (AA), poly(vinylpyrrolidone) (PVP, $M_w \approx 55,000$) were purchased from Aldrich. 10% Pd/C and 20% Pt/C were obtained from Alfa Aesar. High pure argon (Ar, 99.999%) was obtained from Shanghai Weichuang Standard Gas Company. Vulcan XC-72R carbon was obtained from Cabot Company. All chemicals were used without any further purification.

Synthesis of the PdCu Intermetallic Nanoparticles

For the synthesis of the cubic PdCu nanoparticles, a modified literature procedure was used. Typically, 0.1 mmol of $\text{Pd}(\text{acac})_2$, 0.4 mmol of $\text{CuCl}_2 \cdot 2\text{H}_2\text{O}$ and 1.2 mmol of TPP were dissolved into 5 mL of oleylamine in three-neck round bottom flask equipped

with a condenser and attached to a Schlenk line. The reaction system was purged of argon at least by three cycles of evacuation. Under the argon atmosphere, the flask was immersed in an oil bath at 80 °C for 20 min until the reaction mixture turned into the transparent blue liquid. Then, the flask was transferred to the oil bath at 170 °C immediately. The blue liquid turned yellow after a few minutes and became black finally. The reaction system kept this temperature for 4 hours before it cooled to room temperature naturally in the air. The black powder was washed and separated by dispersing the reaction mixture in 2 mL chloroform and 10 mL ethanol, followed by centrifugation at 7000 rpm for 5 min.

The preparation process for spherical PdCu nanoparticles is similar to that of cubic PdCu particles. The amount of the TPP and oleylamine increased to 1.5 mmol and 8 mL. The black powder was washed firstly by centrifugation at 500 rpm for 3 min to remove some larger particles. Then, the liquid supernatant was washed by the same method of the PdCu cubes.

The final products were dispersed in chloroform for further characterization.

Synthesis of the Pd Cubes

According to the previous reported method, 105 mg of PVP, 60 mg of AA, 300 mg of KBr, and 8.0 mL of DI water were mixed in a 20 mL glass vial. The mixture was preheated to 80 °C for 10 min to dissolve all chemicals. Then 3 mL of prepared Na₂PdCl₄ in OLA (75 mg for Na₂PdCl₄) was quickly injected into the preheated solution before the reaction kept 80 °C for 3 h. After the solution cooled to room temperature, the precipitate was washed with ethanol and acetone by centrifugation at 10000 rpm for 3 times, and then re-dispersed in ethanol for further use.

Acknowledgements

The work is sponsored by National Key R&D Program of China (No.2017YFB0406000 and 2017YFA0303403), the National Science Foundation of China (21875137, 61974042, 51521004, and 51420105009), Innovation Program of Shanghai Municipal Education Commission (Project No. 2019-01-07-00-02-E00069), the 111 Project (Project No. B16032), and fund from Center of Hydrogen Science and Joint Research Center for Clean Energy Materials at Shanghai Jiao Tong University for financial supports. H.Z. acknowledges the financial support from Shanghai Automotive Industry Corporation (1714) and the computing resources from Shanghai Jiao Tong University Supercomputer Center. We also thank ECNU Multifunctional Platform for Innovation (004) for characterization support.

Conflict of Interest

The authors declare no conflict of interest.

Keywords: electrocatalysts · intermetallic phases · nanoparticles · oxygen reduction reaction · peroxide reduction

- [1] J. Wu, H. Yang, *Acc. Chem. Res.* **2013**, *46*, 1848–1857.
- [2] Z. Peng, H. Yang, *Nano Today* **2009**, *4*, 143–164.
- [3] M. Shao, Q. Chang, J. P. Dodelet, R. Chenitz, *Chem. Rev.* **2016**, *116*, 3594–3657.
- [4] J. Wu, J. Zhang, Z. Peng, S. Yang, F. T. Wagner, H. Yang, *J. Am. Chem. Soc.* **2010**, *132*, 4984–4985.
- [5] J. Wu, L. Qi, H. You, A. Gross, J. Li, H. Yang, *J. Am. Chem. Soc.* **2012**, *134*, 11880–11883.
- [6] X. Tian, X. Zhao, Y. Su, L. Wang, H. Wang, D. Dang, B. Chi, H. Liu, E. J. M. Hensen, X. W. Lou, B. Y. Xia, *Science* **2019**, *366*, 850–856.
- [7] A. Chalgin, F. Shi, F. Li, Q. Xiang, W. Chen, C. Song, P. Tao, W. Shang, T. Deng, J. Wu, *CrystEngComm* **2017**, *19*, 6964–6971.
- [8] Y. Ma, W. Gao, H. Shan, W. Chen, W. Shang, P. Tao, C. Song, C. Addiego, T. Deng, X. Pan, et al., *Adv. Mater.* **2017**, *29*, 1–8.
- [9] J. Wu, A. Gross, H. Yang, *Nano Lett.* **2011**, *11*, 798–802.
- [10] J. Wu, H. Yang, *Nano Res.* **2011**, *4*, 72–82.
- [11] F. Li, Y. Qin, A. Chalgin, X. Gu, W. Chen, Y. Ma, Q. Xiang, Y. Wu, F. Shi, Y. Zong, et al., *ChemistrySelect* **2019**, *4*, 5264–5268.
- [12] M. Luo, Z. Zhao, Y. Zhang, Y. Sun, Y. Xing, F. Lv, Y. Yang, X. Zhang, S. Hwang, Y. Qin, et al., *Nature* **2019**, *574*, 81–85.
- [13] D. Wang, H. L. Xin, Y. Yu, H. Wang, E. Rus, D. A. Muller, H. D. Abruña, *J. Am. Chem. Soc.* **2010**, *132*, 17664–17666.
- [14] F. Liao, T. W. B. Lo, S. C. E. Tsang, *ChemCatChem* **2015**, *7*, 1998–2014.
- [15] M. Shao, T. Yu, J. H. Odell, M. Jin, Y. Xia, *Chem. Commun.* **2011**, *47*, 6566.
- [16] T. C. Nagaiah, D. Schäfer, W. Schuhmann, N. Dimcheva, *Anal. Chem.* **2013**, *85*, 7897–7903.
- [17] G. J. DeYulia, J. M. Cárcamo, O. Bórquez-Ojeda, C. C. Shelton, D. W. Golde, *Proc. Natl. Acad. Sci. USA* **2005**, *102*, 5044–5049.
- [18] Y. Zhang, M. Janyasupab, C.-W. Liu, P.-Y. Lin, K.-W. Wang, J. Xu, C.-C. Liu, *Int. J. Electrochem.* **2012**, *2012*, 1–8.
- [19] B. D. Adams, C. K. Ostrom, A. Chen, *J. Electrochem. Soc.* **2011**, *158*, 434–439.
- [20] X. Sun, S. Guo, Y. Liu, S. Sun, *Nano Lett.* **2012**, *12*, 4859–4863.
- [21] B. Li, J. Prakash, *Electrochem. Commun.* **2009**, *11*, 1162–1165.
- [22] L. Arroyo-Ramírez, R. Montano-Serrano, T. Luna-Pineda, F. R. Román, R. G. Raptis, C. R. Cabrera, *ACS Appl. Mater. Interfaces* **2013**, *5*, 11603–11612.
- [23] M. Neergat, V. Gunasekar, R. Rahul, *J. Electroanal. Chem.* **2011**, *658*, 25–32.
- [24] M. H. Shao, K. Sasaki, R. R. Adzic, *J. Am. Chem. Soc.* **2006**, *128*, 3526–3527.
- [25] Y. Dai, P. Yu, Q. Huang, K. Sun, *Fuel Cells* **2016**, *16*, 165–169.
- [26] J. Wu, S. Shan, J. Luo, P. Joseph, V. Petkov, C. J. Zhong, *ACS Appl. Mater. Interfaces* **2015**, *7*, 25906–25913.
- [27] J. Mao, Y. Liu, Z. Chen, D. Wang, Y. Li, *Chem. Commun.* **2014**, *50*, 4588–4591.
- [28] W. P. Wu, A. P. Periasamy, G. L. Lin, Z. Y. Shih, H. T. Chang, *J. Mater. Chem. A* **2015**, *3*, 9675–9681.
- [29] Y. Yang, C. Dai, D. Wu, Z. Liu, D. Cheng, *ChemElectroChem* **2018**, *5*, 2571–2576.
- [30] Z. Yin, W. Zhou, Y. Gao, D. Ma, C. J. Kiely, X. Bao, *Chem. Eur. J.* **2012**, *18*, 4887–4893.
- [31] L. Zhang, S. Il Choi, J. Tao, H. C. Peng, S. Xie, Y. Zhu, Z. Xie, Y. Xia, *Adv. Funct. Mater.* **2014**, *24*, 7520–7529.
- [32] X. Wu, Q. Xu, Y. Yan, J. Huang, X. Li, Y. Jiang, H. Zhang, D. Yang, *RSC Adv.* **2018**, *8*, 34853–34859.
- [33] A. Dasgupta, R. M. Rioux, *Catal. Today* **2019**, *330*, 2–15.
- [34] Y. Yan, J. S. Du, K. D. Gilroy, D. Yang, Y. Xia, H. Zhang, *Adv. Mater.* **2017**, *29*, 1605997.
- [35] C. Wang, D. P. Chen, X. Sang, R. R. Unocic, S. E. Skrabalak, *ACS Nano* **2016**, *10*, 6345–6353.
- [36] K. Jiang, P. Wang, S. Guo, X. Zhang, X. Shen, G. Lu, D. Su, X. Huang, *Angew. Chem. Int. Ed.* **2016**, *55*, 9030–9035; *Angew. Chem.* **2016**, *128*, 9176–9181.
- [37] Y. Qiu, L. Xin, Y. Li, I. T. McCrum, F. Guo, T. Ma, Y. Ren, Q. Liu, L. Zhou, S. Gu, et al., *J. Am. Chem. Soc.* **2018**, *140*, 1–20.
- [38] C. Wang, X. Sang, J. T. L. Gamler, D. P. Chen, R. R. Unocic, S. E. Skrabalak, *Nano Lett.* **2017**, *17*, 5526–5532.
- [39] L. Zhang, F. Hou, Y. Tan, *Chem. Commun.* **2012**, *48*, 7152–7154.
- [40] J. T. L. Gamler, A. Leonardi, H. M. Ashberry, N. N. Daanen, Y. Losovyj, R. R. Unocic, M. Engel, S. E. Skrabalak, *ACS Nano* **2019**, *13*, 4008–4017.
- [41] D. Wu, C. Dai, S. Li, D. Cheng, *Chem. Lett.* **2015**, *44*, 1101–1103.
- [42] Q. Gao, Y. Ju, D. An, M. Gao, C. Cui, J. Liu, H.-P. Cong, S.-H. Yu, *ChemSusChem* **2013**, *6*, 1878–1882.
- [43] M. Jin, H. Liu, H. Zhang, Z. Xie, J. Liu, Y. Xia, *Nano Res.* **2011**, *4*, 83–91.
- [44] M. Shao, J. H. Odell, S. Il Choi, Y. Xia, *Electrochem. Commun.* **2013**, *31*, 46–48.

- [45] S. Rudi, C. Cui, L. Gan, P. Strasser, *Electrocatalysis* **2014**, *5*, 408–418.
- [46] J. Greeley, I. E. L. Stephens, A. S. Bondarenko, T. P. Johansson, H. A. Hansen, T. F. Jaramillo, J. Rossmeisl, I. Chorkendorff, J. K. Nørskov, *Nat. Chem.* **2009**, *1*, 552–556.
- [47] X. Li, L. An, X. Wang, F. Li, R. Zou, D. Xia, *J. Mater. Chem.* **2012**, *22*, 6047–6052.
- [48] Y. Xiong, H. Shan, Z. Zhou, Y. Yan, W. Chen, Y. Yang, Y. Liu, H. Tian, J. Wu, H. Zhang, et al., *Small* **2017**, *13*, 1603423.
- [49] J. Wu, P. Li, Y. T. Pan, S. Warren, X. Yin, H. Yang, *Chem. Soc. Rev.* **2012**, *41*, 8066–8074.
- [50] F. Xiao, Y. Li, X. Zan, K. Liao, R. Xu, H. Duan, *Adv. Funct. Mater.* **2012**, *22*, 2487–2494.
- [51] M. Luo, Y. Sun, Y. Qin, S. Chen, Y. Li, C. Li, Y. Yang, D. Wu, N. Xu, Y. Xing, et al., *Chem. Mater.* **2018**, *30*, 6660–6667.
- [52] H. S. Wroblowa, Y.-C. Pan, G. Razumney, *J. Electroanal. Chem. Interfacial Electrochem.* **1976**, *69*, 195–201.
- [53] N. M. Marković, T. J. Schmidt, V. Stamenković, P. N. Ross, *Fuel Cells* **2001**, *1*, 105–116.
- [54] J. K. Nørskov, J. Rossmeisl, A. Logadottir, L. Lindqvist, J. R. Kitchin, T. Bligaard, H. Jónsson, *J. Phys. Chem. B* **2004**, *108*, 17886–17892.
- [55] Y. Sha, T. H. Yu, B. V. Merinov, W. A. Goddard, *ACS Catal.* **2014**, *4*, 1189–1197.
- [56] W. Zhang, G. Fan, H. Yi, G. Jia, Z. Li, C. Yuan, Y. Bai, D. Fu, *Small* **2018**, *14*, 1703713.

Manuscript received: March 9, 2020

Revised manuscript received: April 27, 2020

Accepted manuscript online: May 5, 2020